DOI 10.1007/s10527-019-09850-y
Biomedical Engineering, Vol. 52, No. 6, March, 2019, pp. 371-378. Translated from Meditsinskaya Tekhnika, Vol. 52, No. 6, Nov.-Dec., 2018, pp. 6-10.
Original article submitted October 18, 2018.

Scientific Grounds for the Design of Electrical Impedance Systems for Monitoring the Parameters of Central Hemodynamics and Respiration

I. K. Sergeev[1,2]

Among the instrumented methods for assessing the volume characteristics of cardiac activity, ultrasound, MRI, and CT with contrast are well known. Conventional methods do not provide for measurement of the parameters of central hemodynamics and respiration in monitoring conditions. The possibility of multichannel electrical impedance technology allows the stroke volume and fractional output of the heart to be determined and the displacement of the ventricular walls to be visualized in real time with an accuracy no worse than 1-2 mm. This article considers questions of the implementation of techniques for computing stroke and minute volumes of the circulation and displacements of the heart chamber by solving the electrical impedance measurement problem. Results of mathematical and physical modeling of cardiac activity based on precordial measurements are presented.

Introduction

Data from a WHO report [1] indicate that heart diseases cause the death of about 17 million people around the world each year, which is about 29% of all deaths. Of these, 7.2 million people die from ischemic heart disease and 5.7 million as a result of stroke. On average, early diagnosis of cardiovascular impairments decreases mortality to 70%. The development of instrumented technologies for the early detection of hemodynamic abnormalities is an effective tool for decreasing mortality due to this nosology.

Interest in electrical impedance methods declined from the moment of the wide introduction of MRI, CT, and ultrasound technologies into clinical practice. This was due to the initially poor characteristics of the recording apparatus, which did not allow the task of determining hart activity parameters to be solved as well as by MRI and CT. The possibility of investigating hemodynamic parameters not only of the heart overall but also of its parts (ventricles, valves, atria, displacement of the apex of the heart) set out in the works of Pushcarr (1959), along with transthoracic rheography, opened up the potential for increasing the diagnostic value of impedance technologies [2, 3]. To date, the limitations of electrical impedance technologies have not allowed spatial resolution or more than 1-2 mm.

The technical capacities of multichannel electrical impedance recording devices now provide spatial resolution competing with that of other widely used instrumented methods [4, 5].

Studies performed during the period 1999-2017 at the scientific school of the Bauman Moscow State Technical University yielded the results underlying the technology. Instruments such as the "Rheocardiomonitor" and the REO-32 provide for research and the creation of methods for multichannel electrical impedance mapping of cardiac activity with calculation of central hemodynamic parameters [6, 7].

The main results of these studies were:

– evidence-based design requirements for multichannel impedance measurement transducers and cable systems;

[1] Russian Scientific and Research Institute for Medical Engineering, Federal Service for Surveillance in Healthcare, Moscow, Russia; E-mail: sergeevik@rambler.ru
[2] Bauman Moscow State Technical University, Moscow, Russia.

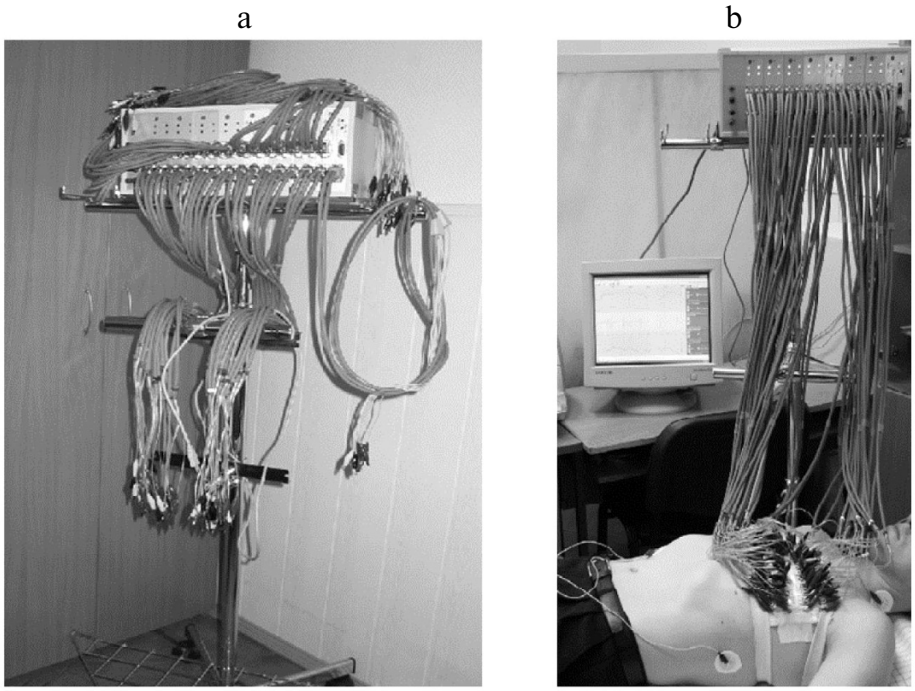

Fig. 1. Impedance measuring system REO-32 (a) and illustration of its experimental use (b) (electrode system).

– a method for metrological testing and calibration, including criteria and procedures supporting the accuracy of the impedance transducer;

– evidence-based criteria for selection, classification, and validation of rheocycles;

– a method for determining hemodynamic phases;

– calculated ratios for determining hemodynamic parameters in cardiology patients;

– a method for extracting the respiratory pattern and analyzing central hemodynamic parameters during the respiratory phases;

– technology for multichannel axial-transverse electrical impedance mapping;

– evidence-based parameters, construction and positioning of electrode systems with consideration of the depth of insertion and individual features of the location of the heart for determining displacements of the cardiac chamber;

– confirmation that the accuracy of determination of hemodynamic parameters on the basis of electrical impedance measurements is no less than that of MRI or ultrasound.

The REO-32 multichannel impedance measurement system (Fig. 1) meets the requirements for solving the problems of electrical impedance measurements, including dynamic visualization of cardiac activity, which is a variety of electrical impedance tomography (EIT).

The EIT method is carried out on reconstructions of the conductivity or dielectric permeability of a body part using a set of surface electrical measurements.

The electrodes are positioned on the body surface. Alternating currents (50-150 kHz) of low amplitude (acting values of up to 5 mA) are passed through current electrodes, and potential electrodes are used to record changes in tension, which are proportional to changes in impedance. In the frequency range 50-150 kHz, the tangent of the angle of the dielectric losses to the environment amounts to less than 10%, which in this case indicates a predominance of the conductivity current over the displacement current [7].

Applications of EIT include monitoring of lung functions [8, 10], diagnosis of breast tumors [11], locating epileptic foci, visualizing the cerebral circulation [12], and visualizing the activity of the heart and major arterial vessels [13]. Until recently, technical solutions were generally experimental systems lacing commercial implementation.

However, in 2011 Draeger (Germany) presented the first commercial product, the Pulma Vita 500 EIT, for dynamic visualization of lung function and monitoring respiratory parameters [14]. The ELISA 800VIT (from Swisstom, Switzerland) is a similar system entering the market at the same time [15]. The invention of EIT as a

medical imaging method is usually attributed to John G. Webster (1978) [16], though the first report of the practical application of an EIT system was published by Barber and Brown (1984) [17].

Important elements in posing the problem for studies were the formation of the biophysical model allowing parameters to be determined in the area of the measurements zone and correct solution of the inverse impedancemetry problem. There was a need to overcome the limitations on the singularity of the solution on the basis of data on hemodynamic properties and the anatomical structure of the heart and chest cage [7, 18].

Techniques and Methods

In the general case, the probing area is a multilayered medium consisting of biological tissues such as muscle, lung tissue, and myocardium, along with blood. Lung tissue covers most of the heart, except for the so-called dull zone, where this tissue is absent. The heart is least covered by lung tissue on exhalation, and the apex of the heart is positioned higher than in inhalation because of the position of the diaphragm; at the exhalation phase, the specific resistances of lung and muscle tissue are similar in magnitude [7, 19].

Analysis of echocardiography and MRI images of the heart shows that the shape of the surface of the internal walls of the myocardium, covering both ventricles at both the end and beginning of mechanical systole, is nearly spherical [10] (Fig. 2, a and b). On this basis, formation of the biophysical model can be based on a two-layer computational model with a spherical inclusion, which is in good agreement with the anatomical structure of the chest cage in the signal recording zone [20]. An illustration of the biophysical model and signal recording scheme is shown in Fig. 2, c and d.

MRI studies were carried out at the A. N. Bakulev Scientific Center of Cardiovascular Surgery using a Siemens Magnetom Avanto tomograph (Germany). The specific resistance of the spherical inclusion in the framework of this model was taken as equal to the specific

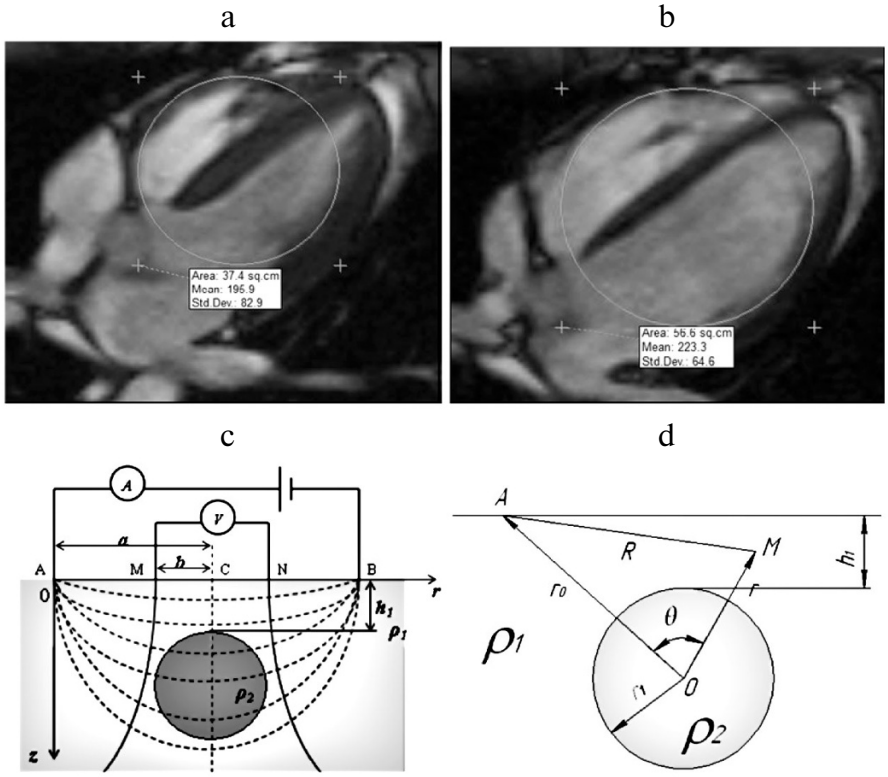

Fig. 2. MRI slices along the long axis of the heart (left) (a) and at the beginning of mechanical systole (right) (b); signal recording scheme and illustration of spherical two-layered model of the chest cage (c); diagram showing calculation of the distribution of potential in the spherical model for point current source (d).

resistance of blood, which for a normal hematocrit is 135 Ω·cm at a probe current frequency of 100 kHz.

In the general case, the function of the field created by the electrode currents (Fig. 2c) satisfies the Laplace equation. For the model used here, there is an analytical solution for the function Z_{MN} [21]. Potentials are calculated for a constant current, without consideration of displacement currents in biological tissues. The analytical solution of the problem of the distribution of impedance on the surface for the model (Fig. 2c) is described by Eq. (1):

$$Z_{MN} = \frac{2 \cdot \rho_1 \cdot b}{\pi \cdot (a^2 - b^2)} + dZ(\rho_1, \rho_2, a, b, r_1, h_1, x, y). \quad (1)$$

The constant part of the impedance corresponds to a uniform medium with specific resistance ρ_1 and the variable part is linked with changes in impedance due to introduction of the spherical inclusion.

As shown by the solution, impedance on the surface depends on the parameters of the geometry of the electrode system and those of the layers: ρ_1 is the effective specific resistance of the first layer, Ω·m; ρ_2 is the specific resistance of blood, Ω·m; a and b are the half-distances between the current and potential electrodes, m; h_1 is the depth of insertion of the spherical inclusion, m; r_1 is the radius of the inclusion, m; and x and y are the displacements of the inclusion relative to the center of the electrode system, m.

Biophysical Modeling

The task of electrical impedance visualization of cardiac activity can be formulated as a task of dynamic determination of the displacements of the boundaries of the heart and its sections. For this model, these displacements can be simplified as two types of movement:

– movement of the center of the sphere (center of mass of the equivalent sphere);

– changes in the radius of the sphere.

The parameters of the model (ρ_1, ρ_2, h_1, r_1, x, y) at fixed electrode system parameters (a, b) require six measurements of impedance and solution of a system of the same number of nonlinear equations. Considering the fact that measurement involves errors in calculating the parameters of the model, solution of these equations does not ensure singularity of the solution, leading to the need to seek approaches to establishing limits on the singularity of the solution.

With the aim of reducing the number of unknowns, preliminary measurements can be made and parameters of the model (h_1, r_1, x, y) determined by CT, MRI, and ultrasound. The sizes of the electrode systems used for electrical impedance measurements were selected on the basis of the condition that the probing depth was comparable with the depth of insertion of the spherical inclusion or the thickness of the first layer, such that h_1, the depth of insertion of the inclusion, is comparable with the distance $2a/3$, where a is the half-distance between the current electrodes, m [19].

ρ_1 can be determined using the apparent resistances method, i.e., the specific resistance of a uniform medium giving the same impedance as that in the present model [18]. ρ_b is determined on the basis of Eq. (2).

For a two-layer model with a spherical inclusion, the relationship between impedance and the parameters of the model can be described functionally using Eq. (3), which is analogous to Eq. (1). Impedance Z_{MN} is used to recompute the specific resistance with Eq. (3) to obtain relationship (4):

$$\rho_b = \frac{\pi \cdot (a^2 - b^2)}{2 \cdot b} \cdot Z_{MN}; \quad (2)$$

$$Z_{MN} = Z(\rho_1, \rho_2, a, b, r_1, h_1, x, y); \quad (3)$$

$$\rho_b = \rho_b(Z_{MN}, \rho_2, a, b, r_1, h_1, x, y). \quad (4)$$

Solution of Eq. (1) to determine ρ_1 is analogous to Eq. (5), which allows ρ_1 to be determined using the values of the measured impedance Z_{MN}:

$$\rho_1 = \rho_1(Z_{MN}, \rho_2, a, b, r_1, h_1, x, y). \quad (5)$$

Methods and Algorithms

Experiments were performed using electrode systems with linear sizes comparable to the probing depth for the first layer [19]. With small electrode assembly dimensions (a, b), the apparent specific resistance ρ_b for the spherical model, like the planar two-layer model, essentially coincides with the specific resistance of the first layer ρ_1, and in this case the probed medium can be regarded as uniform. With larger electrode assembly dimensions (a, b), ρ_b decreases because the current lines pass through a more conductive inclusion – the sphere.

A method was proposed to decrease methodological error in computing ρ_1 using paired measurements of the resistance of the surface layer. According to this hypothesis, the specific resistances of the first layer for the pair of measurements made from a single recording zone with

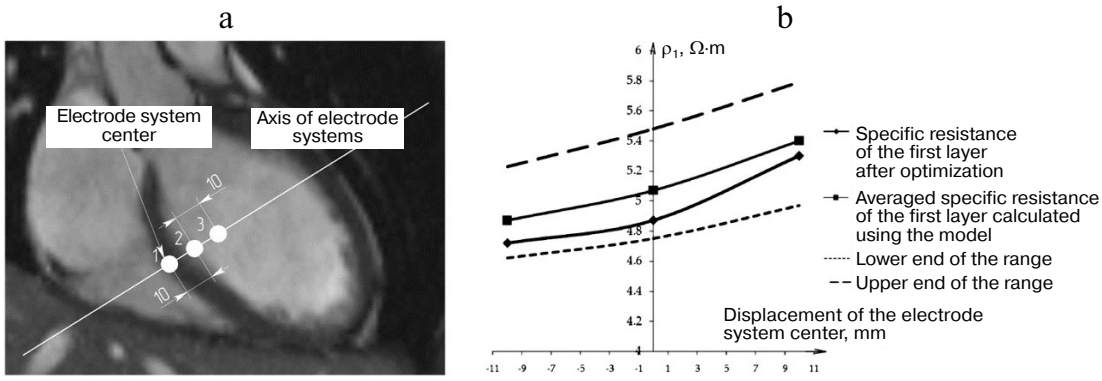

Fig. 3. Illustration of values of specific resistance of the first layer ρ_1 before and after correction (b) calculated at positions 1, 2, and 3 (a).

electrode assembles with different geometrical sizes should coincide when probing depths are similar. The sizes of the electrode systems were selected such that the probing depth was comparable with the depth of insertion of the spherical inclusion h_1. Electrode systems in which the current electrodes were separated by 80, 100, 120, and 140 mm and the potential (measuring) electrodes were separated by 40, 50, 60, and 70 mm respectively were used.

To decrease the effects of the layers through which the probe current passes on the result of computing ρ_1, measurements were made in the dull zone [17, 20]. With this approach, the methodological error of calculating ρ_1 using Eq. (5) for pairs of measurements from a uniform recording zone decreases. As shown by the results, the electrode pressure depth in the measurement zone has significant effects on the result of calculating ρ_1, which needs to be considered in determining ρ_1. The method, allowing solutions to be corrected for multiple relationships, $\rho_b(h_1)$, with recalculation of model (5) to the range of possible changes $a_1 \pm 2$ mm and $a_2 \pm 2$ mm is proposed.

The criterion for correction was criterion (6), which reflects the condition that the solutions for ρ_1 calculated using model (5) are equal for pairs of measurements (Fig. 3a). The result of optimization is a single solution for the pair (a_1, a_2) from the multitude of possible realizations of model (5), see Table 1.

$$\Delta\rho_1(a_1, a_2) = \left[\rho'_1(Z'_{MN}, \rho_2, a_1, b_1, r_1, h_1, x, y) - \right.$$
$$\left. - \rho''_1(Z''_{MN}, \rho_2, a_2, b_2, r_1, h_1, x, y)\right]^2 \to 0. \qquad (6)$$

Additional criterion (7) can be provided by the hypothesis that electrode system dimensions follow a normal distribution law:

$$\left(\Delta a_1^2 + \Delta a_2^2\right) \to \min. \qquad (7)$$

Calculation of the specific resistance of the first layer ρ_1 using model (5) without optimization gave an average increase to 4% (see Table 1). In some cases, deviations in values of ρ_1 could reach 12.5% (see Fig. 3b).

Validation Results

The development of the method requires use of the correct geometrical model for recording displacement of the boundaries and center of mass of the heart.

TABLE 1. Values for Z_{MN} and Specific Resistance of the First Layer ρ_1 Before and After Optimization for Experimental Measurement Series

Position No.	1			2			3		
Dimensions (a, b), mm	Z_{MN}, Ω	ρ_1, Ω·m	ρ_1 (opt.), Ω·m	Z_{MN}, Ω	ρ_1, Ω·m	ρ_1 (opt.), Ω·m	Z_{MN}, Ω	ρ_1, Ω·m	ρ_1 (opt.), Ω·m
(80, 40)	49	4.8	4.72	51.65	5.08	4.87	53.9	5.3	5.3
(100, 50)	37.5	4.62		38.5	4.75		40.25	4.97	
(120, 60)	32.6	4.84		33.6	5		37.2	5.55	
(140, 70)	30.1	5.23		31.5	5.48		32.2	5.79	

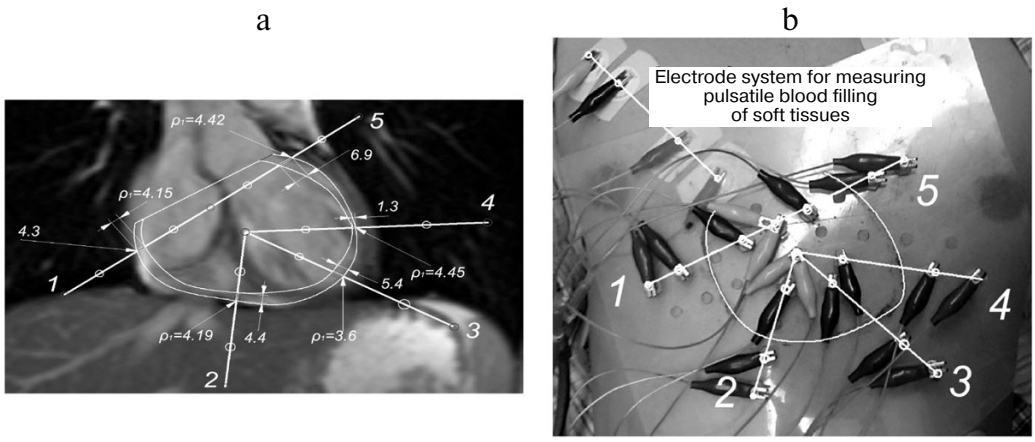

Fig. 4. Illustration of recorded displacements of the boundaries of the heart (a), mm; ρ_1 (Ω·m) values in the displacement recording zones and electrode system positioning scheme used in the experiments (b).

Determination of local displacements in sections Δr_1 using model (1), taking account of criteria (6) and (7), could be made using just five paired signal recording channels in the corresponding anatomical zones of the heart: one zone at the apex of the heart, two zones at the margins in the transverse plane on the left and right in the projection of the heart onto the thoracic cage, and two zones on the margins at an angle of 45° between the apex and the lateral boundaries [18, 20]. Figure 4 shows a scheme for electrical impedance recording of displacements of the boundaries of the heart.

The method developed here decreased the relative error of determinations of ρ_1 to 3% and the error of determination of Δr_1 to 5%.

Equation (8) was used to compute Δr_1, and this is analogous to Eq. (1):

TABLE 2. Experimental Values for Specific Resistance of the First Layer ρ_1 and Displacements Δr_1

Position No.	1	2	3	4	5
Dimensions (a, b), mm	(80, 40)	(80, 40)	(100, 50)	(100, 50)	(80, 40)
Experiment 1. Male 26 years, normosthenic, h_1 in the range 18-22 mm					
ρ_1 (opt.), Ω·m	4.15	4.19	3.6	4.45	4.42
Δr_1, mm; h_1 = 20 mm	2	2.7	2.6	0.6	3.4
Δr_1, mm; h = 18 mm	1.7	2.3	2.2	0.5	2.8
Δr_1, mm; h = 22 mm	2.4	3.1	3	0.7	4.1
Error in Δr_1, mm	0.7	0.8	0.8	0.2	1.3
Experiment 2. Male 26 years, hypersthenic, h_1 about 37 mm					
ρ_1 (opt.), Ω·m	9.26	8.13	9.52	10.2	11.77
Δr_1, mm; h_1 = 37 mm	4.1	5.6	2.6	2.7	4.6
Δr_1, mm; h = 35 mm	3.5	4.8	2.3	2.4	4.1
Δr_1, mm; h = 39 mm	4.7	6.1	3.1	2.9	4.9
Error in Δr_1, mm	0.6	0.5	0.5	0.2	0.3

$$Z_{MN} = \frac{2 \cdot \rho_1 \cdot b}{\pi \cdot (a^2 - b^2)} + dZ\left[\rho_1(t), \rho_2, a, b, r_1, h_1, x, y\right]. \quad (8)$$

In contrast to Eq. (1), $\rho_1(t)$ in Eq. (8) was regarded as a function of pulsatile blood filling of the soft tissues, which for tissues of the first layer is uniform and falls within the recording zone. Recording of $\rho_1(t)$ in the experiment was performed with an additional electrode assembly (Fig. 4b) located on the free zone on the left; $\rho_1(t)$ included the constant ρ_1 and pulsatile $\Delta\rho_1$ components [19]; h_1 in the parameters of model (1) was determined from MRI data. Depending on the phase of respiration, the range of changes in h_1 between the inhalation and exhalation phase averaged ±2 mm.

Computations of SV were performed geometrically on the basis of the truncated cone method for two depths of insertion of the heart h_1. In experiment 1, with h_1 = 18 mm, the computed change in heart volume was 38 mL, while at h_1 = 22 mm it was 48 mL. Calculation of the change in volume for the two values of h_1 came from the need to assess the influence of h_1 measured by MRI on the accuracy of determination of stroke volume. In experiment 2, the change in cardiac volume for h_1 = 35 mm was 80 mL and that for h_1 = 39 mm the change was 103 mL. These data correspond to the output volumes of the left and right ventricles of the heart. Stroke volumes of the heart in experiment 2 were 40 and 52 mL respectively.

Computational experiments showed that on average, a 20% error level in determining h_1 led to a 24% determination error for stroke volume. MRI studies showed that during ejection, the center of mass was displaced, this making a contribution to the change in stroke volume though it was not considered in these calculations. This is needed to correct computation of the displacement Δr_1 using Eq. (8).

Conclusions

This technology allows changes in the geometrical sizes of the equivalent spheres Δr_1 to be determined with error levels of no more than 5% and provides compensation for calculation errors in h_1 arising as a result of pressure of the electrode system in the recording zone.

Analysis of the sensitivity of model (1) showed that the error level in determining the radius of the equivalent sphere r_1 (m) of 1% in the error budget of Δr_1 was no more than 0.4%, which is negligible. Experimental measurements and calculations showed that changes in impedance in the range 50-150 mΩ correspond to changes in the linear dimensions of Δr_1 of 1-5 mm.

These results allowed development of the technology for dynamic visualization of heart activity with accuracy of no worse than 1-2 mm. The main factors influencing the accuracy of recording impedance signals were determined, along with the error budget in calculations of hemodynamic parameters and visualization of displacements of the boundaries of the heart.

The study results showed that the error in assessing hemodynamic parameters for the contingent of men (normosthenics) was no greater than 15-20%, which is comparable to the natural level of variability.

These results allow multichannel electrical impedance technologies to be positioned as a diagnostic method suitable for most clinical applications.

REFERENCES

1. http://www.who.int/mediacentre/factsheets/fs317/ru/ (accessed October 22, 2018).
2. Pushcarr, U. T., "Precordial rheocardiography and its clinical value," Terap. Arkh., No. 9, 57-62 (1959).
3. Pushcarr, U. T., "Pulmonary, aortic and precordial rheography in heart insufficiency and in patients with pulmonary arterial hypertension," Am. Heart J., **1**, 34-38 (1961).
4. Pekker, Ya. S., Brazovskii K. S., and Usov, V. N., Electrical Impedance Tomography [in Russian], NTL, Tomsk (2004).
5. Korzhenevskii, A. V., Kornienko, V. N., and Kul'tiasov, M. Yu., "Electrical impedance computerized tomography for medical applications," PTE, No. 3, 133-140 (1997).
6. Shchukin, S. I., Zubenko, V. G., Belyaev, K. R., and Morozov, A. A., "Rheocardiomonitoring systems," Biomed. Radioelektr., No. 3, 46-60 (1999).
7. Sergeev, I. K., Safonova, L. P., and Shchukin, S. I., "A system and technology for multichannel impedance mapping of the biomechanical activity of the heart," Biomed. Radioel., No. 10, 4-14 (2010).
8. Gurevich, M. I. et al., Impedance Rheoplethysmography [in Russian], Naukova Dumka, Kiev (1982).
9. Nguyen, D. T., Jin, C., Thiagalingam, A., and McEwan, A. L., "A review on electrical impedance tomography for pulmonary perfusion imaging," Physiol. Meas., **33**, No. 5, 695-706 (2012).
10. Pikkemaat, R., Tenbrock, K., Lehmann, S., and Leonhardt, S., "Electrical impedance tomography: New diagnostic possibilities using regional time constant maps," Appl. Cardiopulm. Pathophysiol., **16**, 212-225 (2012).
11. Korzhenevskii, A. V., Karpov, A. Yu., Kornienko, V. N., Kul'tiasov, Yu. S., and Cherepenin, V. A., "An electrical impedance tomography system for three-dimensional visualization of breast tissue," Biomed. Tekhnol. Radioel., No. 8, 5-10 (2003).
12. Adey, W. R., Kado, R. T., and Didio, J., "Impedance measurements in brain tissue of animals using microvolt signals," Exp. Neurol., **5**, 47-66 (1962).
13. Brown, B. H., Barber, D. C., and Seagar, A. D., "Applied potential tomography: Possible clinical applications," Clin. Phys. Physiol. Meas., **1**, 109-121 (1985).
14. http://www.draeger.com/sites/ru_ru/Pages/Hospital/PulmoVista-500.aspx?navID=289 (accessed October 22, 2018).
15. http://www.swisstom.com/en/products/elisa-800vit-2 (accessed October 22, 2018).

16. Henderson, R. P. and Webster, J. G., "An impedance camera for spatially specific measurements of the thorax", IEEE Trans. Biomed. Eng., **25**, 250-254 (1978).
17. Brown, B. H. and Barber, D. C., "Applied potential tomography (review article)," J. Phys. E: Sci. Instrum., **17**, 723-733 (1984).
18. Kirpichenko, Yu. E., Timokhin, D. P., and Shchukin, S. I., "Assessment of stroke volume and fractional output by electrical impedance mapping of the heart," Biomed. Radioelektr., No. 1, 48-51 (2013).
19. Tikhomirov, A. N., Malakhov, A. I., Shchukin, S. I., Kobelev, A. V., Kudashov, I. A., Maslennikov, M. A., and Petrov, V. I., "Assessment of the effects of specific electrical resistance of the tissues of the upper layer on impedance measurements," Biomed. Radioel., No. 1, 20-24 (2013).
20. Zolotko, Yu. L., Atlas of Human Topographic Anatomy [in Russian], Meditsina, Moscow (1967).
21. Tikhonov, A. N. and Samarskii, A. A., Equations for Mathematical Physics [in Russian], Vysshaya Shkola, Moscow (1994).